



Monitoring aboveground forest biomass dynamics over three decades using Landsat time-series and single-date inventory data

Trung H. Nguyen^{a,b,d,e,*}, Simon D. Jones^{a,b}, Mariela Soto-Berelov^{a,b}, Andrew Haywood^c, Samuel Hislop^{a,b}

^a Remote Sensing Centre, Geospatial Science, School of Science, RMIT University, Australia

^b Cooperative Research Centre for Spatial Information (CRCSI), Australia

^c European Forest Institute, Barcelona, Spain

^d Department of Environment, Land, Water and Planning (DELWP), Victoria, Australia

^e Faculty of Resource Management, Thai Nguyen University of Agriculture and Forestry (TUAF), Vietnam



ARTICLE INFO

Keywords:

Aboveground biomass
Landsat time-series
Forest disturbance
Forest recovery
Single-date inventory
Lidar
Australia

ABSTRACT

Understanding forest biomass dynamics is crucial for carbon and environmental monitoring, especially in the context of climate change. In this study, we propose a robust approach for monitoring aboveground forest biomass (AGB) dynamics by combining Landsat time-series with single-date inventory data. We developed a Random Forest (RF) based kNN model to produce annual maps of AGB from 1988 to 2017 over 7.2 million ha of forests in Victoria, Australia. The model was internally evaluated using a bootstrapping technique. Predictions of AGB and its change were then independently evaluated using multi-temporal Lidar data (2008 and 2016). To understand how natural and anthropogenic processes impact forest AGB, we analysed trends in relation to the history of disturbance and recovery. Specifically, change metrics (e.g., AGB loss and gain, Years to Recovery - Y2R) were calculated at the pixel level to characterise the patterns of AGB change resulting from forest dynamics. The imputation model achieved a RMSE value of 132.9 Mg ha^{-1} ($\text{RMSE\%} = 46.3\%$) and R^2 value of 0.56. Independent assessments of prediction maps in 2008 and 2016 using Lidar-based AGB data achieved relatively high accuracies, with a RMSE of 108.6 Mg ha^{-1} and 135.9 Mg ha^{-1} for 2008 and 2016, respectively. Annual validations of AGB maps using un-changed, homogenous Lidar plots suggest that our model is transferable through time (RMSE ranging from $109.65 \text{ Mg ha}^{-1}$ to $112.27 \text{ Mg ha}^{-1}$ and RMSE% ranging from 25.38% to 25.99%). In addition, changes in AGB values associated with forest disturbance and recovery (decrease and increase, respectively) were captured by predicted maps. AGB change metrics indicate that AGB loss and Y2R varied across bioregions and were highly dependent on levels of disturbance severity (i.e., a greater loss and longer recovery time were associated with a higher severity disturbance). On average, high severity fire burnt from 200 Mg ha^{-1} to 550 Mg ha^{-1} of AGB and required up to 15 years to recover while clear-fell logging caused a reduction in 250 Mg ha^{-1} to 600 Mg ha^{-1} of AGB and required nearly 20 years to recover. In addition, AGB within un-disturbed forests showed statistically significant but monotonic trends, suggesting a mild gradual drop over time across most bioregions. Our methods are designed to support forest managers and researchers in developing forest monitoring systems, especially in developing regions, where only a single date forestry inventory exists.

1. Introduction

Understanding forest biomass dynamics is essential for carbon and environmental monitoring. As forest biomass has a significant influence on the global carbon budget, knowledge of biomass dynamics is crucial to understanding net sources and sinks of terrestrial carbon (Houghton, 2005; Le Toan et al., 2011). In the context of climate change, a

comprehensive understanding of forest biomass dynamics over space and time is required to facilitate the implementation of international agreements and conventions such as the Kyoto Protocol and The United Nations Programme on Reducing Emissions from Deforestation and Forest Degradation (UN-REDD) (Mora et al., 2012; UN-REDD Programme Secretariat, 2013). In particular, a spatial and temporal knowledge of biomass change can support policy-making processes that

* Corresponding author at: Remote Sensing Centre, Geospatial Science, School of Science, RMIT University, Australia.

E-mail address: trung.nguyen3@rmit.edu.au (T.H. Nguyen).

aim to preserve ecosystem integrity in forests and reduce greenhouse gas emissions while simultaneously accommodating and maintaining human needs (Mora et al., 2012; Tomppo et al., 2009).

Forest biomass monitoring and reporting are traditionally dependent on National Forest Inventory (NFI) programs usually deployed through the systematic establishment and measurement of forest ground plots. The implementation of NFI programs, however, is challenging in many forest regions, especially in developing countries which often lack technical, financial and institutional capacity (Tomppo et al., 2009). As a consequence, reporting biomass change through time in these regions is often restricted by having only single-date inventory data that cannot be converted to change estimates. Even where repeat-inventory data are available, they have a very limited spatial coverage which is insufficient to create continuous spatial predictions of forest biomass (Wulder et al., 2004). These problems can be addressed by combining forest inventory with remote sensing data.

The most accurate remote sensing method for predicting forest structure and biomass is obtained with light detection and ranging (Lidar) (Badreldin and Sanchez-Azofeifa, 2015; Cao et al., 2016; Meyer et al., 2013; Pflugmacher et al., 2012; Tsui et al., 2012; Waser et al., 2017; Zald et al., 2014). Lidar data can be used to accurately create forest biomass maps where data are available wall-to-wall (He et al., 2013; Ioki et al., 2014; Meyer et al., 2013; Pflugmacher et al., 2012; Tsui et al., 2012), or to support inventory data by creating Lidar-based plots (White et al., 2016; Wulder et al., 2014) which are then fused with satellite images to map forest biomass and structural attributes across large areas (Bolton et al., 2018; Deo et al., 2017a; Jiménez et al., 2017; Matasci et al., 2018b; Pflugmacher et al., 2014; Zald et al., 2016). Although Lidar has great utility in capturing actual forest structure, Lidar data are generally not available over large areas due to high acquisition costs and advanced computational requirements. Furthermore, Lidar data are unlikely to be available as a time-series to fully capture ecological changes in forests (Kennedy et al., 2018). As a result, current forest biomass monitoring systems for large areas and long-time periods mainly rely on the combination of multi-spectral satellite imagery, such as Landsat time-series, and field-based inventory data.

Landsat satellite data provide a unique opportunity for forest monitoring across large areas and long-time periods. The Landsat archive provides a multi-decadal (since 1972) collection of satellite imagery at a spatial resolution (30 m) sufficient for capturing both natural and anthropogenic changes occurring in forests, from local to land management scales (Cohen and Goward, 2004). The open access of the historic Landsat archive and pre-processed products (e.g., surface reflectance, cloud mask) has facilitated the development of numerous approaches of utilising Landsat time-series imagery in forest monitoring activities (Cohen et al., 2017, 2018; Huang et al., 2010; Kennedy et al., 2010, 2012; Wulder et al., 2018; Powell et al., 2010). Spectral trends and change characteristics derived from temporal analysis of Landsat time-series data have been widely used for wall-to-wall estimations of forest biomass and other structure attributes (e.g., Bolton et al., 2018; Gómez et al., 2014; Kennedy et al., 2018; Main-Knorn et al., 2013; Matasci et al., 2018b; Pflugmacher et al., 2014; Powell et al., 2013; Zald et al., 2016). The extension of estimates through long-time periods has been facilitated by advanced Landsat image processing techniques such as compositing methods (Flood, 2013; White et al., 2014). Image compositing allows users to overcome data anomalies due to cloud cover and scan line errors in Landsat 7 ETM + images by choosing the best available pixel (BAP) from several images (Bolton et al., 2018; Hermosilla et al., 2015; Kennedy et al., 2012; White et al., 2017; Zald et al., 2016). Temporal trajectories of these initial composites, however, often still contain data gaps, noisy pixels and radiometric inconsistencies, which can cause negative impacts on the temporal modelling of forest attributes (Pflugmacher et al., 2012). Therefore, BAP composites are often further processed to fit temporal trends through individual bands, according to the fitted trend of a spectral index such as the normalized burn ratio (NBR) (Matasci et al., 2018a, b; Zald et al.,

2016). The final result is a collection of seamless, radiometrically consistent surface-reflectance composites, which can then be used for temporal predictions of forest attributes, such as aboveground biomass (AGB) (Kennedy et al., 2018; Matasci et al., 2018a).

A commonly used modelling method for relating observed AGB and Landsat data is k-Nearest Neighbour (kNN) imputation (e.g., Beaudoin et al., 2014; Bolton et al., 2018; Kennedy et al., 2018; Matasci et al., 2018b; Ohmann et al., 2014; Zald et al., 2016). This approach is a non-parametric and multivariate modelling method that imputes/shares observed values of forest measurements to target samples (or target pixels) (Hudak et al., 2008). With a single NN ($k = 1$), the imputed value of each target sample is assigned as the observed value of the nearest training sample, resulting in more realistic predictions of forest attributes (Eskelson et al., 2009; Hudak et al., 2008). Recent studies have demonstrated the ability of temporally extending imputation models to estimate forest structure and AGB through time (Deo et al., 2017b; Kennedy et al., 2018; Matasci et al., 2018a). For example, Matasci et al. (2018a) developed a Random Forest (RF) based imputation model combining Landsat data with Lidar plot-derived information to create annual forest structure estimates (1984–2016) across 650 million ha of Canadian forests. In another study, Kennedy et al. (2018) used a Gradient Nearest Neighbour (GNN) imputation method to build a robust empirical forest biomass monitoring system.

In this study, we present a robust approach for estimating forest AGB dynamics across space and time using Landsat time-series and single-date inventory data. The specific objectives are to: (1) demonstrate a modelling method for creating annual forest AGB maps from Landsat time-series and inventory data; (2) evaluate the robustness and transferability of applying a single model through time to estimate AGB dynamics; (3) characterise spatial and temporal patterns of AGB dynamics according to forest disturbance and recovery histories, which can inform jurisdictions as to how these ecological changes impact AGB dynamics. To achieve these objectives, we first develop a RF-based imputation model to consistently create annual maps of AGB across forest areas in Victoria, Australia (7.2 million ha) from 1988 to 2017. Recent studies estimating annual AGB over large areas often combine Landsat data with a large set of re-measured inventory plots (Deo et al., 2017b; Kennedy et al., 2018) or Lidar plots (Matasci et al., 2018a). As such data are often unavailable in many forest regions or countries, this study demonstrates a temporal AGB modelling approach based on sparse single-date forest inventory data. To assess this approach, we used Lidar data to independently validate: (1) annual predictions of AGB, and (2) AGB changes due to disturbance and recovery processes. Finally, to understand how AGB responds to both natural and anthropogenic processes occurring in forests, trends of AGB were analysed according to derived disturbance and recovery histories (Nguyen et al., 2018b).

2. Study area

The study area is found on approximately 7.2 million ha of public land forest estate in the state of Victoria, Australia (Fig. 1). The area spans across 11 of the bioregions, as defined by the Interim Biogeographic Regionalization for Australia (IBRA). These bioregions are distinguished by specific ecological, geological and climatological conditions (Department of Environment and Primary Industries, 2013). The northwest region (Murray Darling Depression) experiences semi-arid conditions, with low to median annual rainfall. Central and western parts of the state such as the Victorian Midlands and Victorian Volcanic Plains are dominated by dry inland conditions. Eastern areas (such as South Eastern Highlands and Australian Alps) reach the highest elevations (up to 2000 m), lowest annual temperatures (3–21 °C), and highest annual rainfall (1800–2500 mm) (BOM, 2019).

The variety of topographic and climatic conditions results in diverse vegetation ecosystems. The north-western region is mostly covered by mallee forests, dominated by small and multi-stemmed woodlands up to

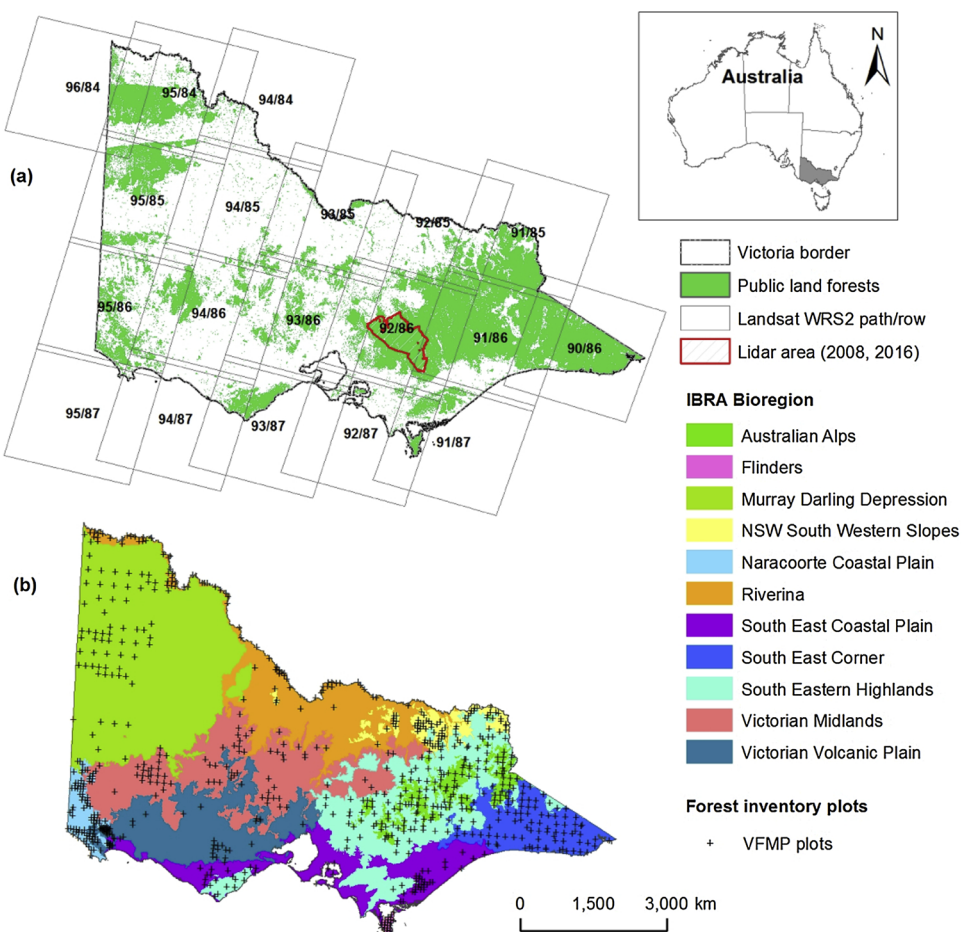


Fig. 1. Study area in Victoria, Australia. (a) The public forest extent, Landsat scenes, and extent of Lidar capture; (b) IBRA bioregions and forest inventory plots from the Victorian Forest Monitoring Program (VFMP).

8 m in height. Box-ironbark and red gum forests are the most common ecosystems in the central parts of the state. They have dense to sparse canopies, up to 25 m in height and grow on flat to undulating topography on rocky and auriferous soils. Covering between the central and eastern parts of the state are damp sclerophyll forests, the most widespread and variable ecosystem in Victoria. Damp sclerophyll forests are found on loam soils, have dense canopies, and reach up to 60 m in height. Eastern Victoria is mostly covered by dry and wet sclerophyll forests. Dry sclerophyll forests include low (up to 25 m) and spreading trees while wet sclerophyll forests are the tallest forest ecosystems in Victoria (able to reach more than 75 m) (Viridans, 2016). Throughout the study period (1988–2017), Victorian forests were mainly impacted by fires, with the largest wildfires occurring during 2003, 2007 and 2009. Logging and other disturbances often occurred within small areas but with a high temporal frequency (Nguyen et al., 2018b).

3. Materials and methods

3.1. Materials

3.1.1. Forest inventory data

Forest inventory plot data included 633 permanent ground circular plots (0.4 ha) measured between 2011–2017 by the Victorian Forest Monitoring Program (VFMP) (Haywood et al., 2016). These plots were randomly selected and stratified by Victoria's 11 bioregions and public tenure (parks and reserves, and State forests). In each plot, numerous measurements were taken on large trees, small trees, herbs and shrubs, and coarse woody debris (see Haywood et al. (2016) for more

information on sampling design and field measurements). For each plot, total AGB was calculated as the sum of live- and dead-standing trees ($> = 10$ cm in diameter at breast height - DBH), small trees (< 10 cm in DBH), stumps, slash and coarse woody debris (i.e., all fallen dead woody material), following Haywood and Stone (2017). AGB values within inventory plots ranged from 0.3 to 1037.7 Mg ha⁻¹, with a mean value of 284.9 Mg ha⁻¹. Following Nguyen et al. (2018a), we also calculated plot-level basal area (BA, m² per ha), and stem density (TD, number of trees per ha) which were then used as response variables in an indirect AGB imputation model.

3.1.2. Lidar-based biomass data

For validating AGB predictions, we used AGB data derived from multi-temporal Lidar data (Nguyen et al., 2019). Airborne Lidar data were acquired by two surveys during the summers of 2008 and 2016, which covered nearly 350,000 ha in the South Eastern Highlands region (Fig. 1). Point cloud data in 2008 were captured using an Optech ALTM 3100 EA sensor with an average density of 0.96 pulses per m² while the data in 2016 were captured by a Trimble AX60 sensor at 4.38 pulses per m². Raw point clouds for each survey were first classified into either ground or non-ground points using an iterative TIN-based method (Isenburg, 2012). A suite of 54 common vegetation metrics was then computed from both Lidar datasets based on the height, density and intensity of the Lidar returns within 30 m × 30 m grid cells, aligning with Landsat pixels. Within the Lidar area, 33 VFMP plots were measured during 2014–2016. A RF model was developed to combine vegetation metrics extracted from the 2016 Lidar and VFMP inventory data. Prior to modelling, the most important Lidar metrics were

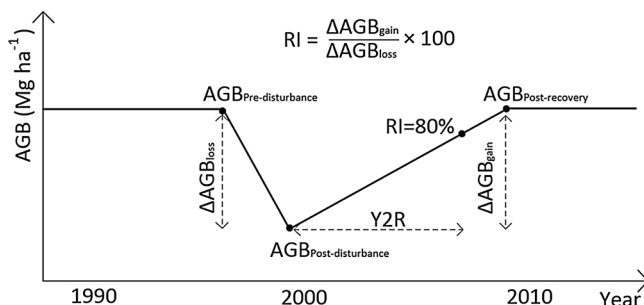


Fig. 2. Change metrics extracted from fitted AGB trajectory.

selected by running a least absolute shrinkage and selection operator (LASSO) model (Efron et al., 2004). Highly correlated variables were also identified and removed. The RF model was evaluated using a leave-one-out cross validation approach and achieved a relatively high accuracy ($\text{RMSE} = 95.09 \text{ Mg ha}^{-1}$, $\text{RMSE\%} = 0.19\%$ and $R^2 = 0.89$). For more details, see Nguyen et al. (2019). The model was then applied to create AGB maps for both years (2008 and 2016) at a spatial resolution of 30 m. For the assessment purpose of this study, we randomly selected 10,000 Lidar plots with the size of 90 m × 90 m (aligning with 3 × 3 Landsat pixels). To minimise potential errors when extracting AGB values using the 3 × 3 pixel window, we selected only those plots that represented homogenous forest areas. This resulted in a set of 8210 plots. The mean AGB values were then extracted for each Lidar plot from the derived maps of 2008 and 2016.

3.1.3. Landsat and forest disturbance data

We processed surface reflectance products (Level-1 Terrain Corrected Landsat TM/ETM + images acquired from January to March inclusive for the years 1988–2017) from the USGS archive for 19 WRS-2 tiles covering the study area (row 84–87, and path 96–90, Fig. 1). Landsat scenes were unpacked, reprojected and applied cloud/shadow masks derived from the Function of Mask (FMASK) algorithm (Zhu and Woodcock, 2012), resulting in a 6-bands LEDAPS image for each Landsat scene. Annual BAP state-wide mosaic composites (hereafter, BAP composites) were computed for the 30-year time-series (1988–2017). For each year, the base image was selected according to its proximity to 15th February, which was chosen as representing a high-stress point of the growth season (Nguyen et al., 2018b).

A forest disturbance dataset for the whole public land forest of Victoria was created following the methods presented in Nguyen et al. (2018b). Briefly, forest change was detected by fitting the NBR time-series (Key and Benson, 2005) using LandTrendr, which is a spectral-temporal segmentation algorithm developed by Kennedy et al. (2010). NBR has been commonly used for forest disturbance and recovery mapping (Kennedy et al., 2012; White et al., 2017). Previous studies also demonstrated that NBR was better than other spectral indices for detecting disturbances occurring in Victorian sclerophyll forests (Hislop et al., 2018b). Maps of disturbance levels (high, medium and low) and causal agents (fire, logging, and others) were created by developing a two-phase classification process using trajectory-derived metrics and a human-interpreted reference dataset (Soto-Berelov et al., 2018). We removed disturbed areas smaller than 0.5 ha using a spatial filter as well as non-forest areas using a forest mask.

The initial BAP composites still contained data gaps and radiometric anomalies which negatively impact temporal predictions of forest attributes (White et al., 2014). We thus generated a suite of synthetic seamless and gap-free composites (hereafter, seamless composites), which have radiometric consistency and no temporal data gaps. To achieve this, the LandTrendr-derived NBR trajectory of each pixel was fitted to the temporal trajectory for each of the six optical bands of the LEDAPS composites, using both point-to-point lines and linear regression (the approach is described in Hislop et al. (2018a)). From annual

Table 1
Internal assessment of the RF-based kNN model via bootstrapping.

Metrics	Mean	Range	STDV
RMSE (Mg ha ⁻¹)	132.9	104.7–168.5	8.6
RMSE% (%)	46.3	42.6–55.2	2.1
R^2	0.56	0.37–0.59	0.05

seamless composites, we calculated NBR, the Tasseled-Cap (TC) components of Greenness (TCG), Wetness (TCW) (Crist, 1985) and Angle (TCA = arctan(TCG/TCB), where TCB is TC Brightness; Powell et al., 2010).

3.2. Aboveground biomass predictions

3.2.1. Model development

We adopted a kNN imputation model (with $k = 1$) which used the RF algorithm, following the findings in Nguyen et al. (2018a). The model searches for the most similar (or the nearest) measured sample and imputes values from that sample to a given target (non-measured) sample (Hudak et al., 2008). The similarity between training and target samples is evaluated based on a non-Euclidean distance metric computed by developing a series of RF models across response variables (one model for each response variable). The RF algorithm computes a proximity matrix where its elements describe the proportion of trees where observations are found in the same terminal nodes (Liaw and Wiener, 2002). The distance metric is derived by subtracting one to that proportion (Crookston and Finley, 2008). For each RF model, the number of trees ($ntree$) was set to 200, and the number of predictor variables selected at each node ($mtry$) was kept as the default (the square root of the number of predictor variables).

Predictor variables included spectral indices (NBR, TCA, TCG and TCW), forest change metrics (disturbance levels, causal agents, and time since disturbance) (Nguyen et al., 2018b), climatic and topographic metrics (elevation, slope, and mean annual rainfall and temperature) (Gallant et al., 2010; Fick and Hijmans, 2017), and pixel locations (northing and easting). Values of predictor variables were extracted from the dates that temporally coincided with field-plot measurement dates, to ensure temporal consistency. The model was trained on two structure variables including total basal area and stem density calculated at the plot-level. The corresponding biomass variable (AGB) associated with the inventory plots were not included in the model but were subsequently attached as ancillary variables to impute to each target pixel. Further descriptions of this biomass modelling approach are presented in Nguyen et al. (2018a).

3.2.2. Annual aboveground biomass predictions

For AGB mapping as well as model assessment (see Section 3.3.1), we processed the model with a non-parametric bootstrapping analysis with 50 repetitions. The selection of this number was a compromise between having a large-enough number of bootstrap replicates while minimizing the processing time required for large area mapping. For each replicate, we implemented the model to produce annual maps of AGB from 1988 to 2017 for all forested pixels within the study area at 30 m spatial resolution. The final predicted value for each pixel was then calculated as the mean of the 50 imputed values derived from the bootstrap replicates.

3.3. Accuracy assessments

The performance of the model was assessed in two ways, internally using bootstrapping analysis and externally using Lidar-based AGB data.

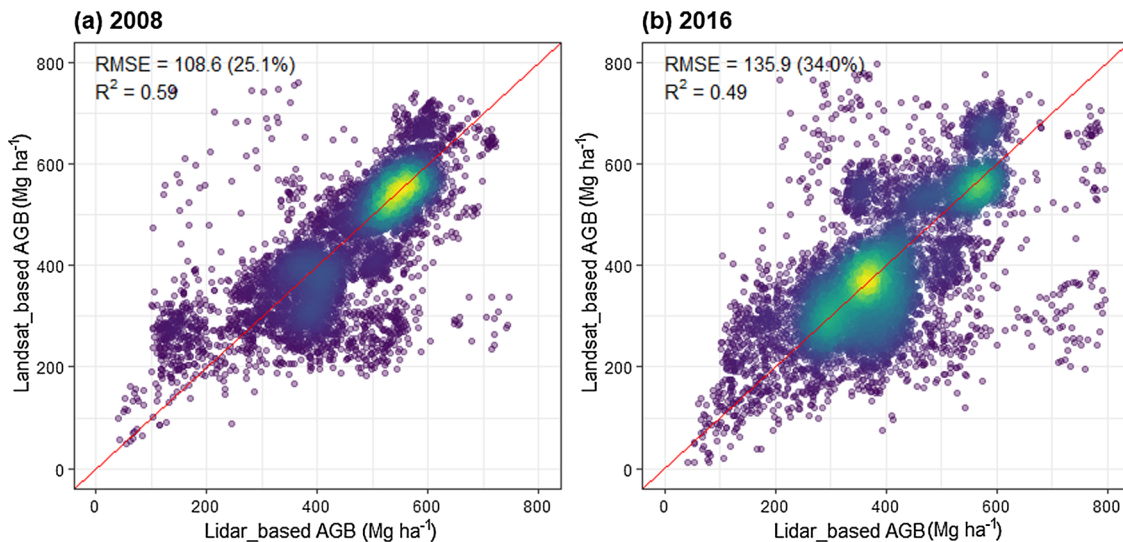


Fig. 3. Relationship between Lidar-based and Landsat-based AGB values across the 8210 validation plots, with the 1:1 line in red. Point density is indicated by a colour gradient from light yellow for high-density to purple for low-density. (For interpretation of the references to colour in this figure legend, the reader is referred to the web version of this article).

3.3.1. Internal assessment via bootstrapping

For each bootstrapping replicate, reference plots (inventory plots) were sampled with replacement, with the sample size set to the number of reference plots (633). About a third of the reference plots were left out of the sample (out-of-bag or OOB) (Crookston and Finley, 2008). The sample was then used as training data in the model while the OOB plots were treated as targets for evaluating model performance. We compared observed and predicted AGB values of OOB plots using the coefficient of determination (R^2), root mean square error (RMSE), and the relative RMSE (RMSE%, RMSE divided by the mean of observed values). The overall performance of the model was assessed by evaluating the mean and range of each of these metrics.

3.3.2. External assessments using Lidar

Annual AGB maps were independently assessed with Lidar AGB plots acquired in 2008 and 2016 (Section 3.1.2). As per the Lidar-based AGB values, Landsat-based AGB values for each plot were extracted as the mean value of a 3×3 pixel window for each year across the time-series.

Three validation approaches were used to validate Landsat-derived AGB predictions. First, we compared Landsat-based to Lidar-based AGB predictions for 2008 and 2016. Second, we conducted a time-series assessment of derived annual AGB maps (1988–2017). To achieve this, we selected a subset of Lidar plots that were homogenous and unchanged throughout the 30-year period. We then calculated the RMSE between Lidar-based AGB values in 2008 and 2016 and used this as a threshold for further filtering. Specifically, only plots whose absolute differences in Lidar-based AGB values between the two years smaller than the defined threshold were selected for further analysis. By doing this, we expected that the temporal variation of AGB values in selected plots was relatively small, so hoped to establish a stable trend. The mean of Lidar-based AGB values in 2008 and 2016 were calculated on per plot basis and compared against Landsat-based AGB values predicted for each year of the time-series. Finally, we evaluated the ability of the developed model in predicting AGB change according to the history of forest dynamics. To do this we integrated Lidar plots with forest disturbance and recovery maps and defined three groups: (1) undisturbed plots; (2) recovery plots (plots experiencing a stand-replacing disturbance prior to 2009 and with an increase in AGB values between 2008 and 2016); and (3) disturbance plots (those experiencing a stand-replacing disturbance between 2009–2016 and with a decrease in AGB values between 2008 and 2016). Changes in AGB values (values in 2016

minus values in 2008) were then independently validated for each group.

3.4. Analysing aboveground forest biomass dynamics

To analyse AGB dynamics according to forest disturbance and recovery processes, we first applied the fitted NBR trajectory to the AGB trajectory. This was achieved using both point-to-point lines and linear regression, similar to the fitting process used for producing annual seamless composites (Section 3.2.1). We then used the fitted trajectory of AGB to characterise spatial and temporal patterns of AGB dynamics according to forest disturbance histories (i.e., disturbance years, severities and agents). In addition, temporal trends of AGB within undisturbed forests were also statistically analysed.

3.4.1. Dynamics within disturbed forests

From the fitted AGB trajectory of each pixel, several change metrics were extracted for each disturbance event to represent AGB change due to disturbance and subsequent recovery processes (Fig. 2). The first two metrics indicated net AGB loss and gain ($\Delta\text{AGB}_{\text{loss}}$ and $\Delta\text{AGB}_{\text{gain}}$), during disturbance and recovery segments, respectively. The net loss was the difference in AGB values between years of post and pre-disturbance while the net gain was the difference between years of post-recovery and post-disturbance. For a disturbed pixel, $\Delta\text{AGB}_{\text{loss}}$ indicated how much AGB was lost due to a disturbance event and $\Delta\text{AGB}_{\text{gain}}$ indicated how much AGB was gained through the consequent recovery process. Relative AGB loss ($r\text{AGB}_{\text{loss}}$) achieved by dividing $\Delta\text{AGB}_{\text{loss}}$ by pre-disturbance value) was also calculated to indicate the percentage of AGB loss from a given disturbance event.

To describe the pattern of post-disturbance recovery, Kennedy et al. (2012) introduced the Recovery Indicator (RI), which scales the magnitude of post-disturbance regrowth to the magnitude of preceding disturbance ($RI = \Delta\text{NBR}_{\text{Regrowth}}/\Delta\text{NBR}_{\text{Disturbance}}$). An adapted form of the metric was also used by White et al. (2017). While previous studies used RI for describing spectral trends (from NBR) of post-disturbance recovery, herein we adopted the metric to represent the recovery pattern of AGB following a disturbance event. Thus, we defined RI as the percentage of AGB gain from post-disturbance recovery ($\Delta\text{AGB}_{\text{gain}}$) in comparison with the amount of AGB loss from a disturbance event ($\Delta\text{AGB}_{\text{loss}}$) (Fig. 2). Lastly, we used the metric Years to Recovery (Y2R), adapted from White et al. (2017) to characterise forest biomass recovery. This metric was defined as the number of years for a given pixel

Table 2

Time-series validation of AGB predictions using un-changed Lidar pixels. The colour ramp dark to light grey corresponds with higher to lower accuracies, respectively.

Year	RMSE (Mg·ha ⁻¹)	RMSE% (%)	R ²
1988	112.08	25.95	0.51
1989	110.39	25.56	0.52
1990	110.55	25.59	0.53
1991	111.34	25.78	0.52
1992	111.16	25.73	0.52
1993	110.13	25.5	0.52
1994	110.84	25.66	0.52
1995	109.98	25.46	0.54
1996	111.09	25.72	0.52
1997	111.38	25.79	0.52
1998	111.2	25.74	0.53
1999	109.74	25.41	0.54
2000	110.41	25.56	0.53
2001	110.15	25.5	0.53
2002	110.47	25.58	0.52
2003	109.65	25.38	0.54
2004	110.57	25.6	0.53
2005	110.69	25.63	0.52
2006	110.37	25.55	0.53
2007	111.77	25.88	0.51
2008	109.83	25.43	0.53
2009	112.27	25.99	0.51
2010	111.85	25.9	0.52
2011	112.16	25.97	0.5
2012	109.73	25.4	0.56
2013	111.04	25.71	0.53
2014	110.43	25.57	0.54
2015	109.74	25.41	0.53
2016	110.02	25.47	0.55
2017	110.43	25.57	0.53
Mean	110.71	25.63	0.52

to reach 80% of its pre-disturbance AGB value (i.e., to obtain a RI value of 80%). Y2R was therefore calculated only for pixels with a RI value equal to or greater than 80%.

Using these metrics, we statistically summarised the spatial and temporal patterns of AGB change to the disturbance history throughout the 30-year period (1988–2017). Total AGB loss and gain (i.e., total $\Delta\text{AGB}_{\text{loss}}$, and $\Delta\text{AGB}_{\text{gain}}$) were calculated for each bioregion and for the state in comparison with disturbance areas. RI was also calculated to examine the balance between total loss and gain at both bioregion and state levels. In addition, temporal trends of total AGB loss were characterised by disturbance agents (fire and logging).

For further characterisations of the relationship between AGB change and forest disturbance history, we randomly selected representative pixels within forest disturbed areas, stratified by bioregions and disturbance levels. At the state level, we grouped these pixels by the classified disturbance levels (high, medium and low). Significant associations, for $\text{rAGB}_{\text{loss}}$ and Y2R across the three disturbance groups, were determined using the Kruskal-Wallis test, a non-parametric one-way ANOVA test (Kruskal and Wallis, 1952). To identify which group was significantly different from each other, multiple

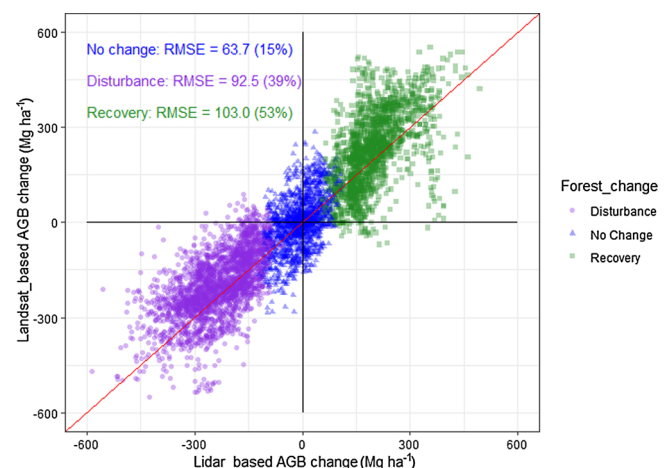


Fig. 4. Validation of AGB change according to the history of forest disturbance and recovery. The 1:1 line is shown in red and the intercept of x and y axes in black. (For interpretation of the references to colour in this figure legend, the reader is referred to the web version of this article).

pairwise-comparisons between disturbance groups were subsequently conducted using the Wilcoxon test (Wilcoxon, 1945). At the bioregion level, sampled pixels were grouped into six disturbance scenarios that were combinations of disturbance causal agents (fire and logging) and disturbance levels (high, medium and low). Groups containing only a small sample with high variability were removed from further analysis. For each bioregion and disturbance scenario, the average of $\Delta\text{AGB}_{\text{loss}}$ and Y2R were calculated. The Wilcoxon tests were also employed to compare and evaluate differences in these values between disturbance groups.

3.4.2. Trends within undisturbed forests

Undisturbed pixel samples over the 1988–2017 period were randomly selected from forested areas. For each bioregion, temporal trends of AGB in undisturbed areas were determined by applying non-parametric Mann-Kendall Trend tests (Libiseller and Grimvall, 2002; Mann, 1945) on the annual time-series of median values of AGB, closely following Matasci et al. (2018a). The test identifies whether there is a significant monotonic trend in AGB time-series ($p < 0.05$). The slope of the trend is determined by the z-statistic value, with a positive or negative value for an increasing or decreasing trend, respectively.

4. Results

4.1. Accuracy assessments

4.1.1. Bootstrapping

Accuracy metrics for the kNN imputation model using the OOB bootstrapping analysis are shown in Table 1. The mean RMSE was 132.9 Mg ha^{-1} , with values ranging from 104.7 Mg ha^{-1} to 168.5 Mg ha^{-1} (standard deviation (STDV) of 8.6 Mg ha^{-1}). The mean RMSE% was 46.3% and ranged from 42.6% to 55.2%. The coefficient of determination R^2 ranged from 0.37 to 0.59, with a mean of 0.56.

4.1.2. External assessments using Lidar-based aboveground biomass

Validation results of AGB predictions for 2008 and 2016 using Lidar plots are shown in Fig. 3. Landsat-based predictions of AGB presented an RMSE of 108.6 Mg ha^{-1} (RMSE% = 25.1%) for 2008 and 135.9 Mg ha^{-1} (RMSE% = 34.0%) for 2016. The R^2 metric was 0.59 for 2008 and 0.49 for 2016. It is clearly evident in the scatterplots that the main distribution area of AGB values in 2008 (around 550 Mg ha^{-1}) was significantly greater than that of 2016 (around 400 Mg ha^{-1}). Most samples fell close to the 1:1 line and within reasonable limits. For both years, there was an overestimation of AGB values in the range of

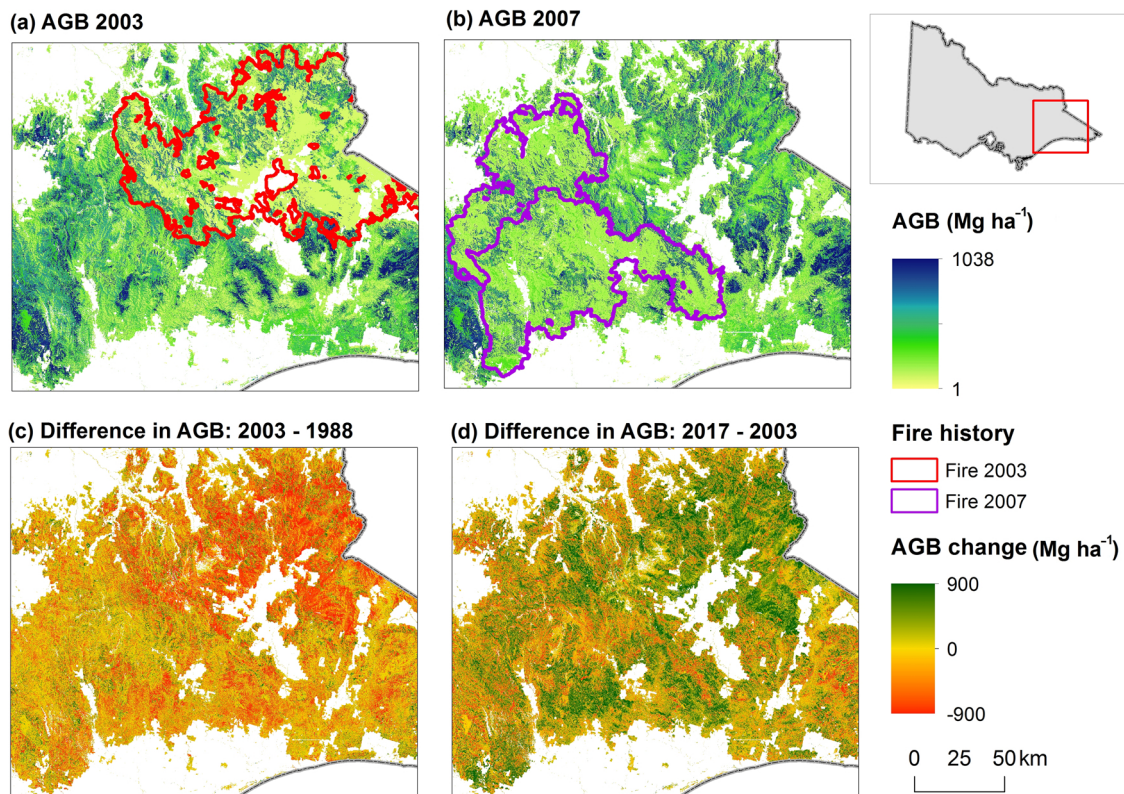


Fig. 5. Predicted AGB maps of 2003 (a) and 2007 (b) in eastern Victoria, Australia; AGB change over 15-year periods: 2003–1988 (c) and 2017–2003 (d).

100–200 Mg ha⁻¹ and an underestimation in the range of 300–500 Mg ha⁻¹.

Annual validations of AGB maps using un-changed Lidar plots achieved relatively high accuracies with a mean RMSE of 110.71 Mg ha⁻¹ (25.63%) and R^2 of 0.52 (Table 2). Annual accuracy metrics were generally stable through time with RMSE values ranging from 109.65 Mg ha⁻¹ (2003) to 112.27 Mg ha⁻¹ (2009) and R^2 from 0.50 (2011) to 0.55 (2012). Years with the highest accuracies were between 2012 and 2016 while the lowest accuracy was obtained during 2009–2011.

The resulting AGB change validation is shown in Fig. 4. AGB change within undisturbed forests was predicted relatively well with a RMSE of 63.7 Mg ha⁻¹ (15.0%). Most of the samples were distributed around the zero value (AGB change = 0) although there were a few outliers (predicting \pm 200–300 Mg ha⁻¹ of AGB change). In addition, a large number of samples had a positive correlation between Lidar-based and Landsat-based predictions of AGB change. Though a small number of samples had a negative correlation (i.e., one increased and the other decreased), values of AGB change within this subset was within a low range.

Predictions of AGB change between 2008 and 2016 according to disturbance and recovery processes obtained a RMSE of 92.5 Mg ha⁻¹ (39.0%) and 103.0 Mg ha⁻¹ (53.0%), respectively (Fig. 4). Forest changes are visible on the scatterplot, as most recovery samples were associated with an increase in AGB and most disturbance samples were associated with a decrease in AGB. Nevertheless, there was a slight overestimation of the increase and underestimation of the decrease (the vast majority of recovery and disturbance samples fell to the left of the 1:1 line).

4.2. Annual aboveground biomass predictions

Annual AGB maps (1988–2017) across Victorian public forests were produced at a 30 m spatial resolution. These spatially explicit products allow us to explore AGB dynamics over large areas. For example, the

difference in AGB for two 15-year periods is shown in Fig. 5. Evidence of large disturbance events (e.g., fires in 2003 and 2007) and associated declines in AGB are clearly evident.

4.3. Aboveground forest biomass dynamics

4.3.1. Dynamics within disturbed forests

AGB change metrics were derived for all disturbed forested pixels across the processing area (Fig. 6). For pixels experiencing multiple disturbance events, change metrics were independently extracted for both the greatest and the second greatest disturbance events. Net AGB loss and gain from the greatest disturbance and subsequent recovery, respectively, are shown in Fig. 6. Because of disturbance, forests lost between 1 Mg ha⁻¹ to 951 Mg ha⁻¹ of AGB and gained between 0 Mg ha⁻¹ to 903 Mg ha⁻¹ of AGB after subsequent recovery. Most disturbed forests (82%) reached pre-disturbance AGB conditions, obtaining a RI value of 80% or greater over a 5–15 years recovery period.

Spatial statistics of AGB dynamics in disturbed areas are shown in Table 3. At the state level, about 6.8e + 08 Mg of AGB has been lost due to disturbance from 1988 to 2017. However, around 95.9% of this loss has been re-gained. The total net loss and gain of AGB at the bioregion level were relatively balanced given that RI values were over 80% (exceptions were the Murray Darling Depression, Victorian Volcanic Plain and Riverina bioregions). Flinders achieved the highest recovery rate (RI = 130%) even though the disturbed area and AGB loss were the lowest. The South Eastern Highlands accounted for approximately half of the total disturbed area and AGB loss across the state (the region has since fully recovered, Fig. 6).

Temporal patterns of AGB loss were generally consistent with annual trends of disturbed area (Fig. 7). On average, fires burned nearly 2.2e + 07 Mg of AGB per year. There were two irregular years, 2003 and 2007, which resulted in 8.2e + 05 ha burned (loss of 1.8e + 08 Mg of AGB) and 1.1e + 06 ha burned (loss of 2.2e + 08 Mg of AGB), respectively. On the other hand, AGB loss resulting from logging events was much lower, about 1.4e + 06 per year, although the first half of the

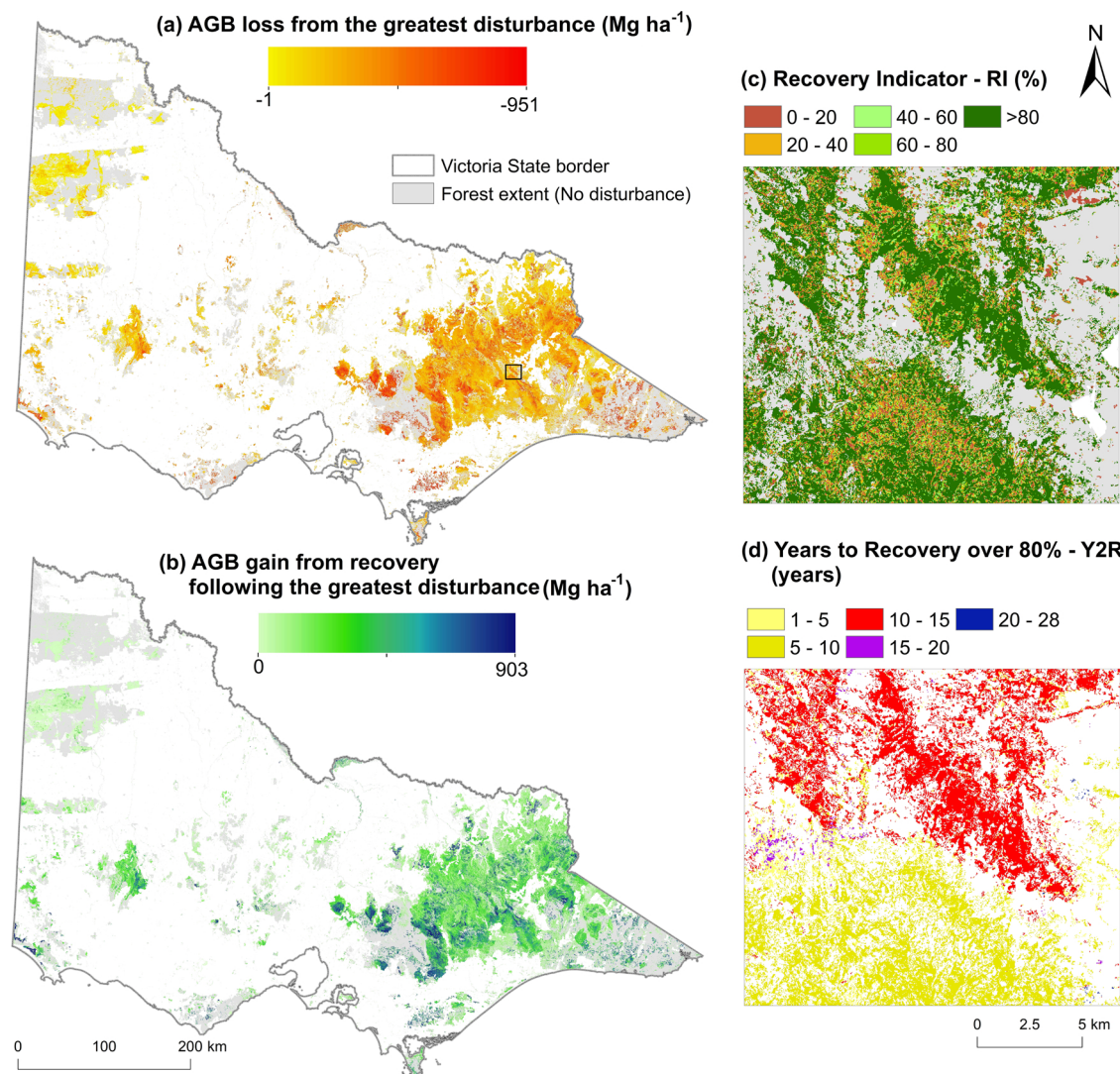


Fig. 6. AGB change metrics across Victoria's public forests during 1988-2017. (a) and (b) show AGB loss and gain ($\Delta\text{AGB}_{\text{loss}}$ and $\Delta\text{AGB}_{\text{gain}}$) as a result of the greatest disturbance and subsequent recovery, respectively. (c) and (d) show the RI and Y2R at a local scale (black box in (a)).

Table 3
Spatial summary of AGB dynamics by bioregion and at the state level during 1988-2017.

Bioregion	Disturbed area (ha)	AGB loss (Mg)	AGB gain (Mg)	RI (%)
Flinders	1.7e + 04	2.0e + 06	2.6e + 06	130.0
Victorian Volcanic Plain	2.0e + 04	2.5e + 06	1.4e + 06	56.0
Riverina	5.4e + 04	8.2e + 06	4.3e + 06	52.4
Naracoorte Coastal Plain	5.6e + 04	5.9e + 06	5.2e + 06	88.1
NSW South Western Slopes	7.1e + 04	8.8e + 06	8.2e + 06	93.2
South East Coastal Plain	7.9e + 04	7.7e + 06	6.2e + 06	80.5
Victorian Midlands	3.4e + 05	4.3e + 07	3.8e + 07	88.8
Murray Darling Depression	4.4e + 05	9.7e + 06	5.8e + 06	59.8
South East Corner	4.7e + 05	8.3e + 07	8.1e + 07	97.6
Australian Alps	5.4e + 05	1.4e + 08	1.2e + 08	85.1
South Eastern Highlands	1.6e + 06	3.8e + 08	3.9e + 08	102.7
State level	3.6e + 06	6.8e + 08	6.6e + 08	95.9

time-series (1990–2003) saw higher rates of loss (recent years have also seen a slight upward trend).

Results from Kruskal-Wallis tests on the representativeness of disturbed pixels indicated significant differences between disturbance levels in both rAGB_{loss} and Y2R ($p < 0.0001$ for both variables, Fig. 8).

Pairwise comparisons using Wilcoxon tests also resulted in significant differences between each pair of disturbance groups ($p < 0.0001$ for all tests). A higher disturbance level was generally associated with a higher loss in AGB greater Y2R.

The means of AGB loss from fires varied across bioregions and

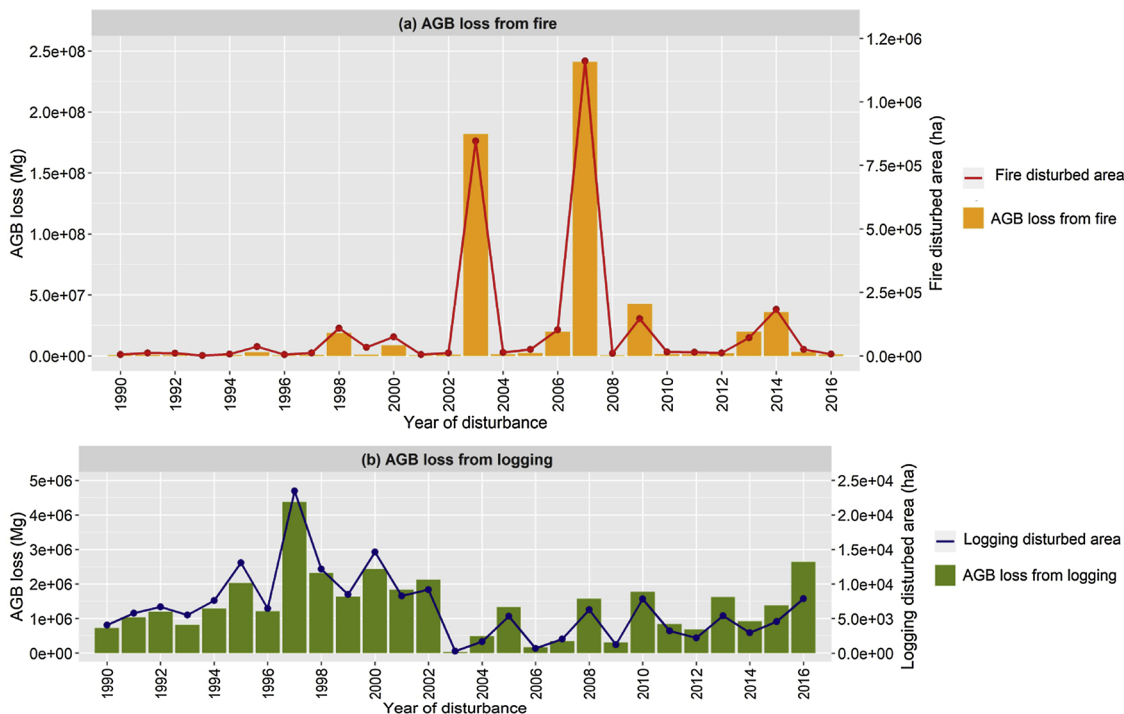


Fig. 7. Temporal patterns of AGB loss caused by (a) fire and (b) logging.

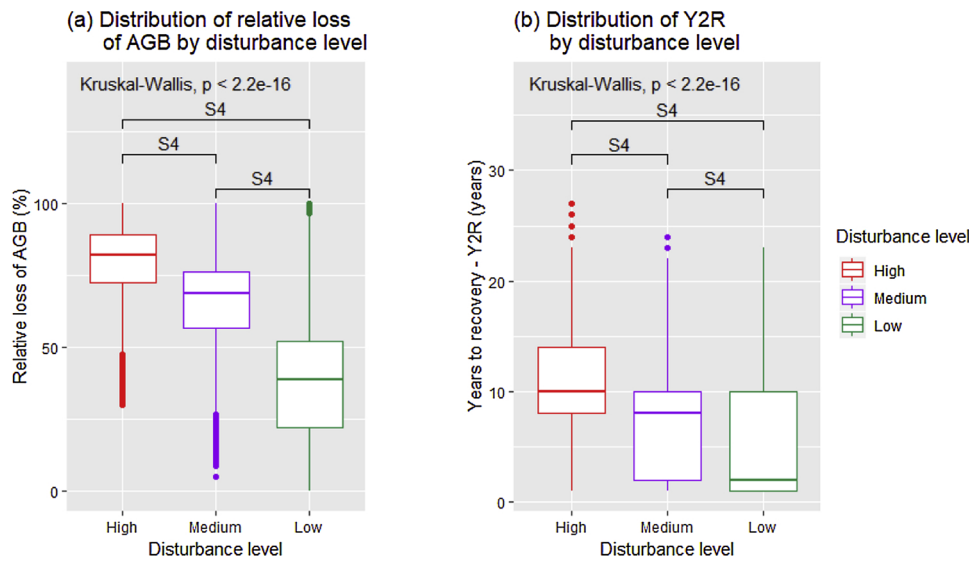


Fig. 8. Distribution of $r\Delta\text{AGB}_{\text{loss}}$ and Y2R by disturbance levels with results from variance tests, (S4 is noted for the significance level of $p < 0.0001$).

disturbance levels (Fig. 9). In the most productive bioregion, the “South East Corner”, fires resulted in the loss of $200\text{--}550 \text{ Mg ha}^{-1}$. The loss of AGB ($\Delta\text{AGB}_{\text{loss}}$) was much lower in less productive bioregions such as Murray Darling Depression and Naracoorte Coastal Plain (from 30 Mg ha^{-1} to 170 Mg ha^{-1}). For all fire-dominated bioregions, a higher severity disturbance generally caused a higher mean of $\Delta\text{AGB}_{\text{loss}}$. Results from the Wilcoxon tests indicated that there were generally significant differences between $\Delta\text{AGB}_{\text{loss}}$ associated with fire disturbance levels ($p < 0.05$ for all tests except in the Murray Darling Depression).

Analysis of Y2R suggested that a higher fire severity was generally associated with a longer recovery duration of AGB (Fig. 9). Most forests required 10–15 years to recover at least 80% of AGB loss after a high

severity fire. On the other hand, the duration for recovery following medium and low severity fires ranged between 5–10 years and 2–3 years, respectively. As with $\Delta\text{AGB}_{\text{loss}}$, the mean values of Y2R associated with each level of fire severity were significantly different from each other ($p < 0.05$ for all Wilcoxon tests).

The patterns of $\Delta\text{AGB}_{\text{loss}}$ and Y2R associated with logging disturbance were similar to those associated with fire disturbance (Fig. 10). Means of $\Delta\text{AGB}_{\text{loss}}$ and Y2R varied across bioregions and were highly dependent on disturbance levels. A higher level of logging generally resulted in a greater value of $\Delta\text{AGB}_{\text{loss}}$ and a longer recovery length. On average, a clear-fell logging event resulted in the loss of $250\text{--}600 \text{ Mg ha}^{-1}$ of biomass, which was similar to high severity fires.

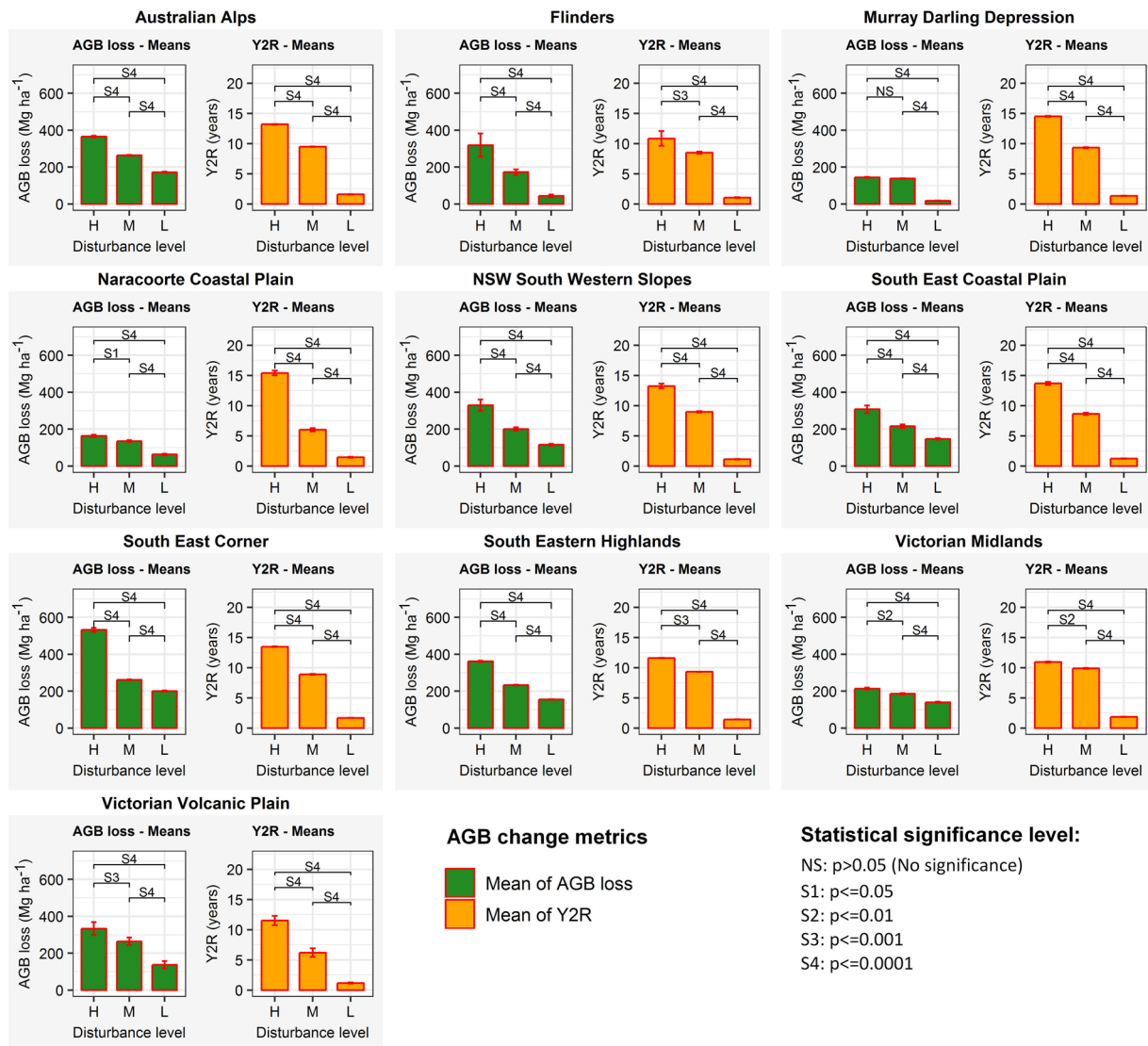


Fig. 9. Means of AGB loss and Y2R associated with fire disturbance across bioregions, with 95% confidence intervals. Notes: H = High, M = Medium, and L = Low disturbance level).

However, 15–19 years was required for recovery following clear-fell logging.

4.3.2. Trends within undisturbed forests

Throughout the 30-year time-series (1988–2017), AGB within undisturbed forests generally followed a monotonic trend across all bioregions (Mann-Kendall trend test produced a p-value of 0), except for the Australian Alps and the Southeast Conner (see Fig. A1 in Appendix A). AGB within undisturbed forests was slightly dynamic. A positive trend ($z < 0$) was found for less productive regions including Murray Darling Depression, Naracoorte Coastal Plain and Flinders while a negative trend ($z > 0$) was common among higher productive bioregions.

5. Discussion

5.1. Biomass modelling approach

This paper presents a robust approach for spatially and temporally estimating AGB dynamics at a land management scale, using single-date

forest inventory plots and an annual Landsat time series (1988–2017). These data sources were combined with a RF-based kNN modelling approach, allowing the extrapolation of single-date measurements of AGB across space and time. Previous studies have built empirical models by combining Landsat time-series with large sets of re-measured inventory plots (Deo et al., 2017b; Kennedy et al., 2018) or Lidar plots (Matasci et al., 2018a). In many forest regions, however, forest inventory plots are often sparse, only measured for a single time period and thus out-of-date. Lidar data, where available, typically covers relatively small areas and is insufficient for creating samples of the forest population. As a comparison, we used 633 single-date inventory plots across 7.2 million ha of forests while Kennedy et al. (2018) used 8454 re-measured plots covering approximately 4.8 million ha of forests in the western US. This makes the work presented herein significantly different from the aforementioned studies.

The modelling method used in this study was found to be the most accurate imputation method for estimating forest AGB from Landsat time-series and field plots in a previous study (Nguyen et al., 2018a). While the kNN model was developed with $k = 1$, the prediction value of each target pixel was calculated as the mean of multiple imputed values

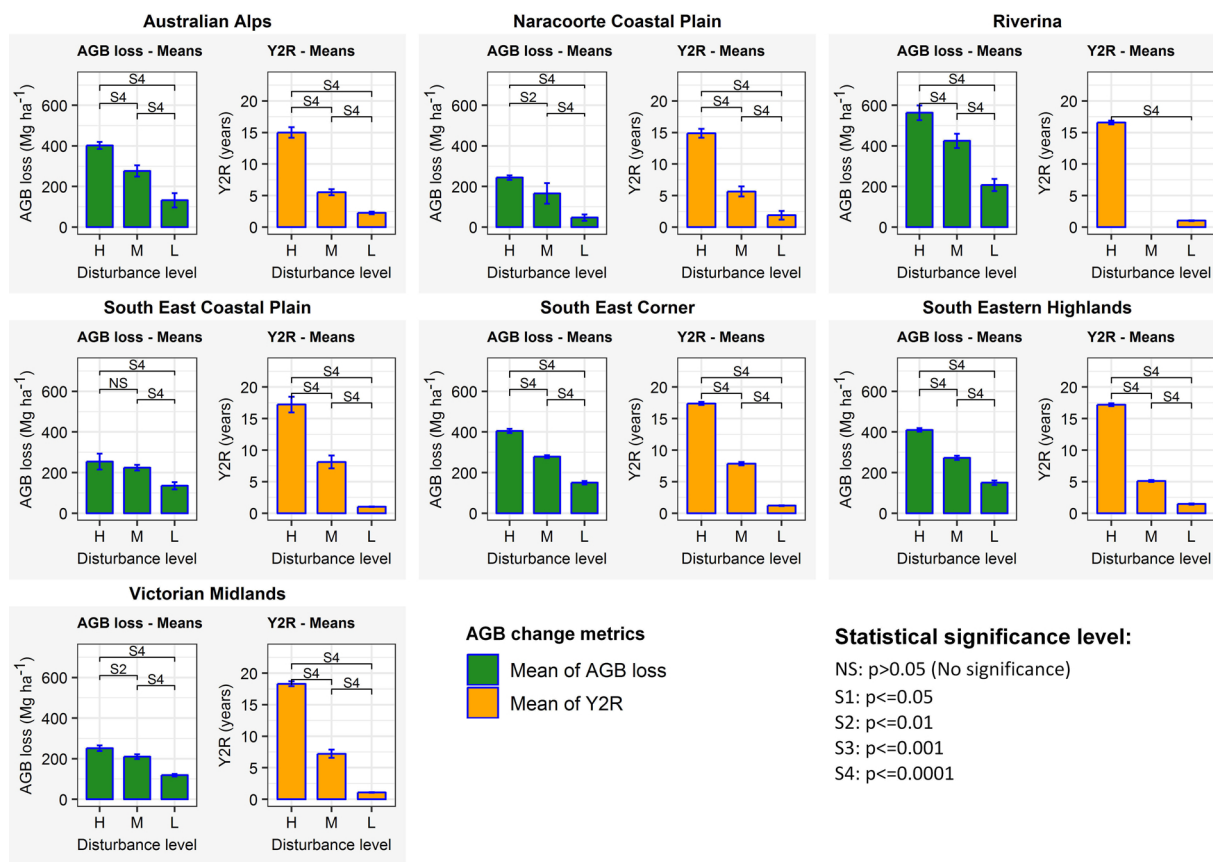


Fig. 10. Means of AGB loss and number of Y2R associated with logging disturbance across bioregions. Notes: H = High, M = Medium, and L = Low disturbance level).

derived using bootstrap iterations. This approach allowed us to reduce the imputation error, in a similar manner to increasing the value of k , while utilising the full range of observed AGB values. When using a $k > 1$, the final prediction value of a given target pixel is the mean of k different observed values associated to the nearest training samples. In contrast, when running the model with replicates, the final prediction value for each target pixel can be a single observed value (when all replicates produced the same imputed value) or the mean of multiple observed values (when replicates produced different imputed values). This approach is particularly useful when a non-standard distribution of biomass values exist in inventory data.

The robustness of our modelling approach was indicated by results from both internal and independent accuracy assessments. Results of the bootstrap validation indicate that the model performance was relatively stable across bootstrap replicates (Table 1), with RMSE ranging from 104.7 Mg ha^{-1} to 168.5 Mg ha^{-1} (STDV = 8.6 Mg ha^{-1}) and R^2 from 0.37 to 0.59 (STDV = 0.05). These results indicated that the imputed values derived from bootstrap replicates for a given pixel (50 values), which were then averaged for the final prediction value, had a low variance.

In addition to bootstrapping analysis, AGB predictions were compared against independent Lidar-based AGB data collected in 2008 and 2016. Both years obtained relatively comparable results (RMSE% value of 25.1% and 34.0% for 2008 and 2016, respectively; Fig. 3). Though some over- and under-estimations were noted, they were within reasonable limits (i.e., close to the 1:1 line), suggesting the model was

transferable when applied through time. The temporal transferability of our model is further confirmed by the results from time-series validation of AGB predictions using un-changed Lidar plots, which indicate stable accuracy over time (Table 2). Slightly lower accuracies found during 2009 to 2011 can be explained by the influence of high-intensity disturbance events occurring within Lidar areas, especially the "Black Saturday" fires in 2009 (Nguyen et al., 2018b), indicating that uncertainties of biomass prediction can be somewhat informed by forest disturbance history. The findings from our time-series validation are consistent with those reported by other studies (Deo et al., 2017b; Matasci et al., 2018a; Powell et al., 2013). As a comparison, Matasci et al. (2018a) predicted annual AGB maps (1984–2016) across Canada's forested ecosystem by integrating Landsat time-series with Lidar plots in a RF-based kNN model. The authors evaluated the model performance using multi-temporal Lidar data collected between 2006 and 2012 in Alberta province and found that the model accuracies were generally stable over time.

The impacts of forest disturbance are clearly evident when comparing the distribution of AGB values between 2008 and 2016, with significant decreases observed (Fig. 3). Results from AGB change validation (Fig. 4) indicate the ability of our modelling approach to capture AGB changes resulting from forest disturbance and recovery processes. Generally, changes in AGB captured by Lidar data were also captured by Landsat-based predictions. It is perhaps not surprising that AGB changes due to disturbance (i.e. decreases) were better estimated than the change resulting from recovery processes (increases), with an RMSE

% of 39.0% and 53.0%, respectively. Many studies have demonstrated that predicting changes associated with forest recovery from spectral data is more challenging than those associated with disturbance (Griffiths et al., 2014; Kennedy et al., 2012; Pickell et al., 2015; White et al., 2017). It is generally straightforward to quantify disturbances as they result in abrupt changes in forest structure (this are normally captured through spectral values). On the other hand, recovery is an ongoing/long-term process and dependent on multiple interacting factors, including the nature of disturbance (severity, agents, and frequency), biological characteristics, and natural conditions (e.g., latitude, climate and topography) (Bartels et al., 2016). In addition, it is established that Landsat spectral signals saturate at relatively low leaf area index and biomass levels, resulting in higher predictions of biomass in the years soon after disturbance (Bartels et al., 2016; Kennedy et al., 2018). This could perhaps explain the slight overestimation of biomass increases as well as the underestimation of biomass decreases indicated in our results. The disturbance samples used in this analysis experienced a stand-replacing disturbance between 2009 and 2016, therefore most of them were on a regrowth trend in 2016. AGB change within undisturbed forests was also captured relatively well with a general agreement between Landsat-based and Lidar-based predictions ($\text{RMSE\%} = 15.0$) though the change was relatively small and complex (both positive and negative correlations, Fig. 4).

5.2. Forest biomass dynamics in relation to disturbance and recovery histories

To effectively support forest management, the analysis of biomass dynamics needs to be consistent with the history of forest disturbance and recovery. While numerous approaches have been used to characterise the patterns of forest biomass dynamics, most of them are sample-based (Matasci et al., 2018a; Powell et al., 2013). In this study, we used change metrics to characterise spatial and temporal patterns of forest AGB across space and time. To a lesser extent, these metrics have been effectively used to represent patterns of forest dynamics at the landscape scale (Kennedy et al., 2012; White et al., 2017). Kennedy et al. (2012) used change magnitude metrics and the recovery indicator (RI) to represent spatial and temporal patterns of forest disturbance and recovery over the period 1985–2008 in the Pacific Northwest region of the United States. Y2R is a robust metric that has been used for characterising the temporal aspect of forest recovery length (Pickell et al., 2015; White et al., 2017). In this study, Y2R suggests that most Victorian forests need 5–15 years to reach pre-disturbance AGB conditions, which corresponds to the findings of Hislop et al. (2019), who estimated Landsat spectral recovery averaged between 4.6–14.7 years in the same study area.

Spatial summaries of AGB change were consistent with the disturbance areas and varied conditions across bioregions (Table 3). Higher change magnitudes (total loss and gain) were generally associated with larger disturbance areas and more productive bioregions (such as Australian Alps and South Eastern Highlands). Overall, the total gain of AGB was slightly lower than the total loss at both state (RI = 95.9%) and bioregion levels (Table 3), which reflects changes from recent disturbances. Statistics of AGB change at the bioregion level indicate the influence of climatic and geological conditions on the return of forest biomass. Regions with the lowest recovery rates (i.e., RI values), such as Victorian Volcanic Plain (54.9%), Riverina (52.0%) and Murray Darling Depression (59.4%), have high annual temperatures and low annual rainfall. We also analysed a 30-year temporal trend of AGB loss from fire and logging disturbances across the study area (Fig. 7). Our results confirm a strong relationship between the amount of AGB loss and disturbance area at the state level regardless of

disturbance causal agents, which is consistent with other studies (Kennedy et al., 2018; Powell et al., 2013). As these statistics are based on spatially and temporally explicit products, they can effectively support decision making processes at a land management scale.

For a forest biomass monitoring system, it is important not only to analyse biomass change across space and time but also to understand how biomass responds to different disturbance scenarios (e.g., severity, causal agent) occurring in forests (Kennedy et al., 2018). By integrating AGB change with defined disturbance causal agents (fire and logging) and severity levels (high, medium and low), we determined AGB loss and recovery length associated with specific disturbance scenarios (Figure 8, 9 and 10). At both state and bioregion levels, we found that the magnitude $\Delta\text{AGB}_{\text{loss}}$ and recovery length (Y2R) were generally dependent on disturbance levels, with higher loss in AGB and longer recovery time for a higher disturbance level. At the bioregion level, results from variance tests indicated that AGB loss and recovery length across disturbance levels were distinguishable from the others (e.g., AGB loss from a low severity fire is significantly lower than from medium and high severity fires). For future AGB monitoring, the mean of AGB loss to each disturbance scenario could be used as “change factors” to calculate forest AGB stock changes at regional scales. Specifically, AGB loss from a subsequent disturbance can be estimated by combining these change factors with the spatial characteristics of change (i.e., disturbance agent and level). Similar to previous studies (e.g., Bartels et al., 2016; Hislop et al., 2019), our results indicate that the recovery length was dependent on not only disturbance characteristics but also climatic and topographic conditions across regions. For regions with harsher environment conditions such as Murray Darling Depression and Naracoorte Coastal Plain, it took an average of 15 years following a disturbance to recover, although the loss of AGB was relatively low (around 180 Mg ha^{-1} , Fig. 9). In addition, results demonstrate that recovery length was generally longer following logging activities than fires. This supports evidence presented in other studies that forests impacted by natural disturbances often recover faster than those impacted by anthropogenic events (Bartels et al., 2016; Cole et al., 2014).

Temporal patterns of AGB on undisturbed forest areas generally followed a monotonic trend excepting the Australian Alps and the Southeast Conner (Fig. A1 in Appendix A). The gradual decrease of AGB in most bioregions may be explained by repeated droughts throughout the last three decades within the study area. Victoria has become warmer and drier since mid-last century and thus forests across the state have been facing an increased risk of declining productivity and tree mortality (Department of Environment and Primary Industries, 2013). An exciting potential future research focus would be on quantifying the impacts of climatic changes on forest biomass dynamics across these areas.

6. Conclusion

This study presents an alternative method for monitoring forest AGB changes over time when multiple date forest inventory and Lidar data are unavailable. We demonstrate an empirical approach for creating annual maps of AGB using Landsat time-series and single-date inventory data over a large area. The robustness of our approach was confirmed by conducting multiple independent validations of AGB estimates using Lidar data. The integration of annual AGB predictions with historical disturbance data allowed us not only to consistently track spatial and temporal patterns of AGB change (loss and gain) resulting from forest dynamics but also to understand how forest AGB responds to specific disturbance scenarios (i.e., disturbance causal agent and magnitude). Our approach can be particularly useful in forest

regions where only single-date and sparse inventory data are available. This can aid forest managers and policy makers in measuring and reporting on forest biomass changes, especially in developing regions.

Acknowledgements

This research was partly funded by the Australian Award Scholarship (AAS) and the Cooperative Research Centre for Spatial

Information (CRCSEI) under Project 4.104 (A Monitoring and Forecasting Framework for the Sustainable Management of southeast Australian Forests at the Large Area Scale). CRCSEI activities were funded by the Australian Commonwealth's Cooperative Research Centres Programme. We also would like to acknowledge the Victorian Department of Environment, Land Water and Planning (DELWP) for providing forest inventory and Lidar data.

Appendix A

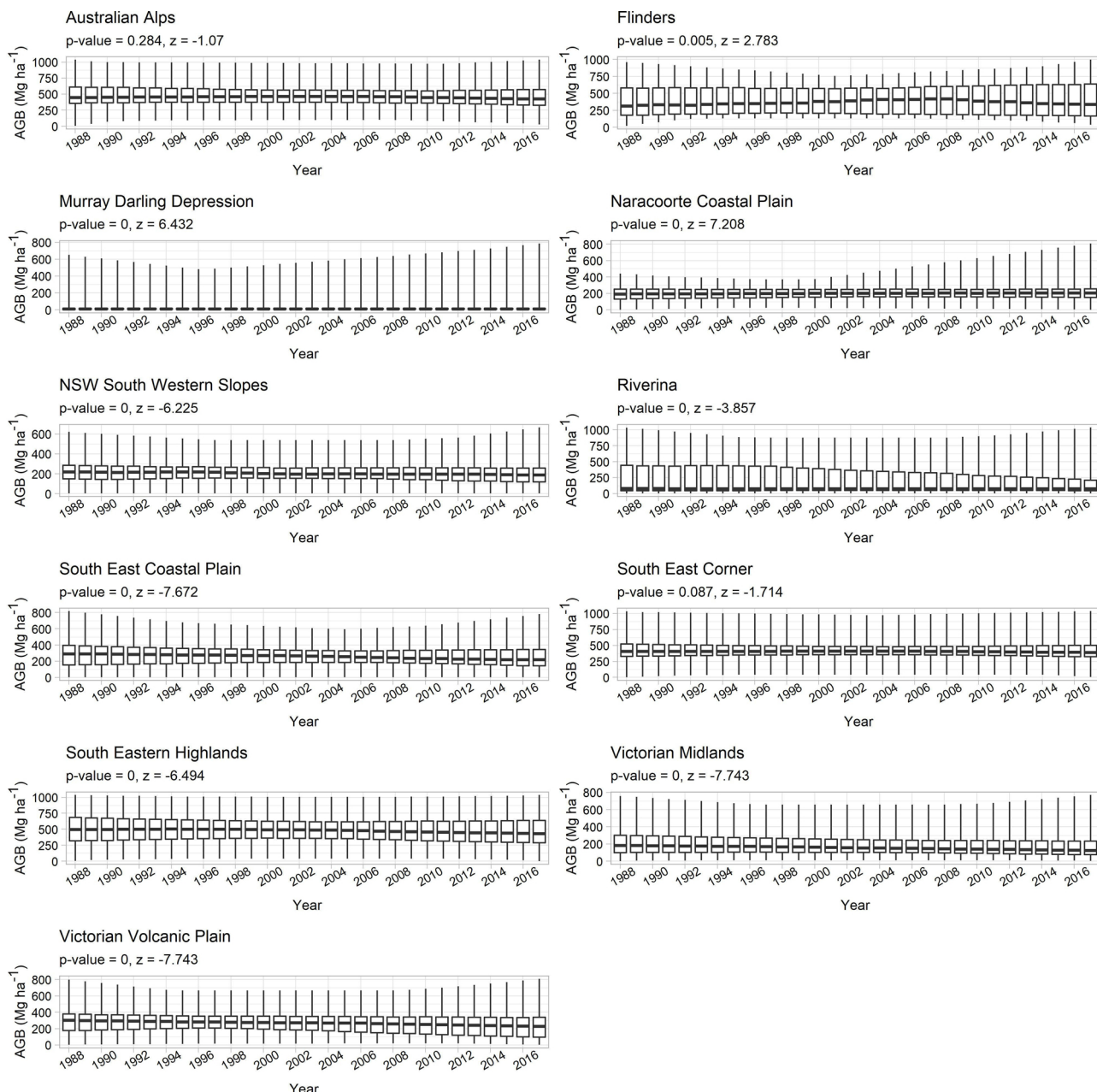


Fig. A1. AGB dynamics in un-disturbed forests across bioregions from 1988 to 2017. p and z statistics are reported by Mann-Kendall trend tests.

References

- Badreldin, N., Sanchez-Azofeifa, A., 2015. Estimating forest biomass dynamics by integrating multi-temporal Landsat satellite images with ground and airborne LiDAR data in the coal valley mine, Alberta, Canada. *Remote Sens. (Basel)* 7, 2832–2849.
- Bartels, S.F., Chen, H.Y.H., Wulder, M.A., White, J.C., 2016. Trends in post-disturbance recovery rates of Canada's forests following wildfire and harvest. *For. Ecol. Manage.* 361, 194–207.
- Beaudoin, A., Bernier, P.Y., Guindon, L., Villemaire, P., Guo, X.J., Stinson, G., Bergeron, T., Magnussen, S., Hall, R.J., 2014. Mapping attributes of Canada's forests at moderate resolution through kNN and MODIS imagery. *Can. J. For. Res.* 44, 521–532.
- Bolton, D.K., White, J.C., Wulder, M.A., Coops, N.C., Hermosilla, T., Yuan, X., 2018. Updating stand-level forest inventories using airborne laser scanning and Landsat time series data. *Int. J. Appl. Earth Obs. Geoinf.* 66, 174–183.
- BOM, 2019. Bureau of Meteorology (BOM). Australian Government, Australia.
- Cao, L., Coops, N.C., Innes, J.L., Sheppard, S.R.J., Fu, L., Ruan, H., She, G., 2016. Estimation of forest biomass dynamics in subtropical forests using multi-temporal airborne LiDAR data. *Remote Sens. Environ.* 178, 158–171.
- Cohen, W., Healey, S., Yang, Z., Stehman, S., Brewer, C., Brooks, E., Gorelick, N., Huang, C., Hughes, M., Kennedy, R., Loveland, T., Moisen, G., Schroeder, T., Vogelmann, J., Woodcock, C., Yang, L., Zhu, Z., 2017. How similar are forest disturbance maps derived from different Landsat time series algorithms? *Forests* 8, 98.
- Cohen, W.B., Goward, S.N., 2004. Landsat's role in ecological applications of remote sensing. *BioScience* 54, 535–545.
- Cohen, W.B., Yang, Z., Healey, S.P., Kennedy, R.E., Gorelick, N., 2018. A LandTrendr multispectral ensemble for forest disturbance detection. *Remote Sens. Environ.* 205, 131–140.
- Cole, L.E., Bhagwat, S.A., Willis, K.J., 2014. Recovery and resilience of tropical forests after disturbance. *Nat. Commun.* 5, 3906.
- Crist, E.P., 1985. A TM tasseled cap equivalent transformation for reflectance factor data. *Remote Sens. Environ.* 17, 301–306.
- Crookston, N.L., Finley, A.O., 2008. *yalImpute*: an R package for kNN imputation. *J. Stat. Softw.* 23, 1–16.
- Deo, R., Russell, M., Domke, G., Andersen, H.-E., Cohen, W., Woodall, C., 2017a. Evaluating site-specific and generic spatial models of aboveground forest biomass based on Landsat time-series and LiDAR strip samples in the Eastern USA. *Remote Sens. (Basel)* 9, 598.
- Deo, R.K., Russell, M.B., Domke, G.M., Woodall, C.W., Falkowski, M.J., Cohen, W.B., 2017b. Using Landsat time-series and LiDAR to inform aboveground forest biomass baselines in Northern Minnesota, USA. *Can. J. Remote. Sens.* 43, 28–47.
- Department of Environment and Primary Industries, 2013. Victoria's State of the Forest Report 2013. Melbourne, Victoria, Australia.
- Efron, B., Hastie, T., Johnstone, I., Tibshirani, R., 2004. Least angle regression. *Ann. Statist.* 32, 407–499.
- Eskelson, B.N.I., Temesgen, H., Lemay, V., Barrett, T.M., Crookston, N.L., Hudak, A.T., 2009. The roles of nearest neighbor methods in imputing missing data in forest inventory and monitoring databases. *Scand. J. For. Res.* 24, 235–246.
- Fick, S.E., Hijmans, R.J., 2017. WorldClim 2: new 1-km spatial resolution climate surfaces for global land areas. *Int. J. Climatol.* 37, 4302–4315.
- Flood, N., 2013. Seasonal composite Landsat TM/ETM+ images using the medoid (a multi-dimensional median). *Remote Sens. (Basel)* 5, 6481–6500.
- Gallant, J.C., Dowling, T.I., Read, A.M., Wilson, N., Tickler, P., Inskeep, C., 2010. Second SRTM Derived Digital Elevation Models User Guide. Geoscience Australia, Canberra, ACT, Australia.
- Gómez, C., White, J.C., Wulder, M.A., Alejandro, P., 2014. Historical forest biomass dynamics modelled with Landsat spectral trajectories. *Isprs J. Photogramm. Remote. Sens.* 93, 14–28.
- Griffiths, P., Kuemmerle, T., Baumann, M., Radloff, V.C., Abrudan, I.V., Lieskovsky, J., Munteanu, C., Ostapowicz, K., Hostert, P., 2014. Forest disturbances, forest recovery, and changes in forest types across the Carpathian ecoregion from 1985 to 2010 based on Landsat image composites. *Remote Sens. Environ.* 151, 72–88.
- Haywood, A., Mellor, A., Stone, C., 2016. A strategic forest inventory for public land in Victoria, Australia. *For. Ecol. Manage.* 367, 86–96.
- Haywood, A., Stone, C., 2017. Estimating large area forest carbon stocks—a pragmatic design based strategy. *Forests* 8, 99.
- He, Q., Chen, E., An, R., Li, Y., 2013. Above-ground biomass and biomass components estimation using LiDAR data in a coniferous forest. *Forests* 4, 984–1002.
- Hermosilla, T., Wulder, M.A., White, J.C., Coops, N.C., Hobart, G.W., 2015. Regional detection, characterization, and attribution of annual forest change from 1984 to 2012 using Landsat-derived time-series metrics. *Remote Sens. Environ.* 170, 121–132.
- Hislop, S., Jones, S., Soto-Berelov, M., Skidmore, A., Haywood, A., Nguyen, T., 2018a. A New semi-automatic seamless cloud-free Landsat mosaicing approach tracks forest change over large extents. *IEEE International Geoscience and Remote Sensing Symposium (IGARSS)*.
- Hislop, S., Jones, S., Soto-Berelov, M., Skidmore, A., Haywood, A., Nguyen, T., 2018b. Using Landsat spectral indices in time-series to assess wildfire disturbance and recovery. *Remote Sens. (Basel)* 10, 460.
- Hislop, S., Jones, S., Soto-Berelov, M., Skidmore, A., Haywood, A., Nguyen, T., 2019. High fire disturbance in forests leads to longer recovery, but varies by forest type. *Remote Sens. Ecol. Conserv. In Press*.
- Houghton, R.A., 2005. Tropical deforestation as a source of greenhouse gas emissions. *Tropical Deforestation and Climate Change.* 13.
- Huang, C., Goward, S.N., Masek, J.G., Thomas, N., Zhu, Z., Vogelmann, J.E., 2010. An automated approach for reconstructing recent forest disturbance history using dense Landsat time series stacks. *Remote Sens. Environ.* 114, 183–198.
- Hudak, A.T., Crookston, N.L., Evans, J.S., Hall, D.E., Falkowski, M.J., 2008. Nearest neighbor imputation of species-level, plot-scale forest structure attributes from LiDAR data. *Remote Sens. Environ.* 112, 2232–2245.
- Ioki, K., Tsuyuki, S., Hirata, Y., Phua, M.-H., Wong, W.V.C., Ling, Z.-Y., Saito, H., Takao, G., 2014. Estimating above-ground biomass of tropical rainforest of different degradation levels in Northern Borneo using airborne LiDAR. *For. Ecol. Manage.* 328, 335–341.
- Isenburg, M., 2012. LAStools-efficient Tools for LiDAR Processing. Available at: <http://www.cs.unc.edu/~isenburg/lastools/> [Accessed October 9, 2012].
- Jiménez, E., Vega, J.A., Fernández-Alonso, J.M., Vega-Nieva, D., Ortiz, L., López-Serrano, P.M., López-Sánchez, C.A., 2017. Estimation of aboveground forest biomass in Galicia (NW Spain) by the combined use of LiDAR, LANDSAT ETM+ and National Forest Inventory data. *iForest Biogeosci.* For. 10, 590–596.
- Kennedy, R.E., Ohmann, J., Gregory, M., Roberts, H., Yang, Z., Bell, D.M., Kane, V., Hughes, M.J., Cohen, W.B., Powell, S., Neeti, N., Larrue, T., Hooper, S., Kane, J., Miller, D.L., Perkins, J., Braaten, J., Seidl, R., 2018. An empirical, integrated forest biomass monitoring system. *Environ. Res. Lett.* 13, 025004.
- Kennedy, R.E., Yang, Z., Cohen, W.B., 2010. Detecting trends in forest disturbance and recovery using yearly Landsat time series: 1. LandTrendr — temporal segmentation algorithms. *Remote Sens. Environ.* 114, 2897–2910.
- Kennedy, R.E., Yang, Z., Cohen, W.B., Pfaff, E., Braaten, J., Nelson, P., 2012. Spatial and temporal patterns of forest disturbance and regrowth within the area of the Northwest Forest Plan. *Remote Sens. Environ.* 122, 117–133.
- Key, C., Benson, N., 2005. Landscape Assessment: Remote Sensing of Severity, the Normalized Burn Ratio and Ground Measure of Severity, the Composite Burn Index. FIREMON: Fire Effects Monitoring and Inventory System Ogden. USDA Forest Service, Rocky Mountain Res. Station, Utah.
- Kruskal, W.H., Wallis, W.A., 1952. Use of ranks in one-criterion variance analysis. *J. Am. Stat. Assoc.* 47, 583–621.
- Le Toan, T., Quegan, S., Davidson, M.W.J., Balzter, H., Paillou, P., Papathanassiou, K., Plummer, S., Rocca, F., Saatchi, S., Shugart, H., Ulander, L., 2011. The BIOMASS mission: mapping global forest biomass to better understand the terrestrial carbon cycle. *Remote Sens. Environ.* 115, 2850–2860.
- Liaw, A., Wiener, M., 2002. Classification and regression by random forest. *R news* 2, 18–22.
- Libiseller, C., Grimvall, A., 2002. Performance of partial Mann–Kendall tests for trend detection in the presence of covariates. *Environmetrics: The official journal of the International Environmetrics Society* 13, 71–84.
- Main-Knorr, M., Cohen, W.B., Kennedy, R.E., Grodzki, W., Pflugmacher, D., Griffiths, P., Hostert, P., 2013. Monitoring coniferous forest biomass change using a Landsat trajectory-based approach. *Remote Sens. Environ.* 139, 277–290.
- Mann, H.B., 1945. Nonparametric tests against trend. *Econometrica: Journal of the Econometric Society* 245–259.
- Matasci, G., Hermosilla, T., Wulder, M.A., White, J.C., Coops, N.C., Hobart, G.W., Bolton, D.K., Tompalski, P., Bater, C.W., 2018a. Three decades of forest structural dynamics over Canada's forested ecosystems using Landsat time-series and lidar plots. *Remote Sens. Environ.* 216, 697–714.
- Matasci, G., Hermosilla, T., Wulder, M.A., White, J.C., Coops, N.C., Hobart, G.W., Zald, H.S.J., 2018b. Large-area mapping of Canadian boreal forest cover, height, biomass and other structural attributes using Landsat composites and lidar plots. *Remote Sens. Environ.* 209, 90–106.
- Meyer, V., Saatchi, S.S., Chave, J., Dalling, J.W., Bohlman, S., Fricker, G.A., Robinson, C., Neumann, M., Hubbell, S., 2013. Detecting tropical forest biomass dynamics from repeated airborne lidar measurements. *Biogeosciences* 10, 5421–5438.
- Mora, B., Herold, M., de Sy, V., Wijaya, A., Verchot, L.V., Penman, J., 2012. Capacity Development in National Forest Monitoring: Experiences and Progress for REDD+. & eds. Center for International Forestry Research (CIFOR), Bogor, Indonesia.
- Nguyen, T., Jones, S., Soto-Berelov, M., Haywood, A., Hislop, S., 2018a. A comparison of imputation approaches for estimating forest biomass using Landsat time-series and inventory data. *Remote Sens. (Basel)* 10, 1825.
- Nguyen, T.H., Jones, S., Soto-Berelov, M., Skidmore, A., Haywood, A., Hislop, S., 2019. Estimate forest biomass dynamics using multi-temporal lidar and single-date inventory data. In: *IEEE International Geoscience and Remote Sensing Symposium (IGARSS)*. Yokohama, Japan.
- Nguyen, T.H., Jones, S.D., Soto-Berelov, M., Haywood, A., Hislop, S., 2018b. A spatial and temporal analysis of forest dynamics using Landsat time-series. *Remote Sens. Environ.* 217, 461–475.
- Ohmann, J.L., Gregory, M.J., Roberts, H.M., 2014. Scale considerations for integrating forest inventory plot data and satellite image data for regional forest mapping. *Remote Sens. Environ.* 151, 3–15.
- Pflugmacher, D., Cohen, W.B., Kennedy, E., 2012. Using Landsat-derived disturbance history (1972–2010) to predict current forest structure. *Remote Sens. Environ.* 122, 146–165.
- Pflugmacher, D., Cohen, W.B., Kennedy, R.E., Yang, Z., 2014. Using Landsat-derived disturbance and recovery history and lidar to map forest biomass dynamics. *Remote Sens. Environ.* 151, 124–137.
- Pickell, P.D., Hermosilla, T., Frazier, J.R., Coops, N.C., Wulder, M.A., 2015. Forest recovery trends derived from Landsat time series for North American boreal forests. *Int. J. Remote Sens.* 37, 138–149.
- Powell, S.L., Cohen, W.B., Healey, S.P., Kennedy, R.E., Moisen, G.G., Pierce, K.B., Ohmann, J.L., 2010. Quantification of live aboveground forest biomass dynamics with Landsat time-series and field inventory data: a comparison of empirical modeling approaches. *Remote Sens. Environ.* 114, 1053–1068. <https://doi.org/10.1016/j.rse.2009.12.018>.
- Powell, S.L., Cohen, W.B., Kennedy, R.E., Healey, S.P., Huang, C., 2013. Observation of

- trends in biomass loss as a result of disturbance in the Conterminous U.S.: 1986–2004. *Ecosystems* 17, 142–157.
- Soto-Berelov, M., Haywood, A., Jones, S.D., Hislop, S., Nguyen, H.T., 2018. Creating robust reference (training) datasets for large area time series disturbance attribution. In: Weng, Q.E. (Ed.), *Remote Sensing: Time Series Image Processing*. Taylor and Francis.
- Tomppo, E., Gschwantner, T., Lawrence, M., McRoberts, R.E. (Eds.), 2009. *National Forest Inventories*. Springer, Dordrecht.
- Tsui, O.W., Coops, N.C., Wulder, M.A., Marshall, P.L., McCardle, A., 2012. Using multi-frequency radar and discrete-return LiDAR measurements to estimate above-ground biomass and biomass components in a coastal temperate forest. *Isprs J. Photogramm. Remote. Sens.* 69, 121–133.
- UN-REDD Programme Secretariat, 2013. National Forest monitoring systems: monitoring and measurement, reporting and verification (M & MRV) in the context of REDD + activities. 7th Meeting of the UN-REDD Programme Policy Board.
- Viridans, 2016. Victorian Ecosystems and Vegetation. <http://www.viridans.com/ECOVEG/>.
- Waser, L., Ginzler, C., Rehush, N., 2017. Wall-to-Wall tree type mapping from country-wide airborne remote sensing surveys. *Remote Sens.* (Basel) 9.
- White, J., Wulder, M., Hobart, G., Luther, J., Hermosilla, T., Griffiths, P., Coops, N., Hall, R., Hostert, P., Dyk, A., 2014. Pixel-based image compositing for large-area dense time series applications and science. *Can. J. Remote. Sens.* 40, 192–212.
- White, J.C., Coops, N.C., Wulder, M.A., Vastaranta, M., Hilkert, T., Tompalski, P., 2016. Remote sensing technologies for enhancing forest inventories: a review. *Can. J. Remote. Sens.* 42, 619–641.
- White, J.C., Wulder, M.A., Hermosilla, T., Coops, N.C., Hobart, G.W., 2017. A nationwide annual characterization of 25 years of forest disturbance and recovery for Canada using Landsat time series. *Remote Sens. Environ.* 194, 303–321.
- Wilcoxon, F., 1945. Individual comparisons by ranking methods. *Biom. Bull.* 1, 80–83.
- Wulder, M., Skakun, R., Kurz, W., White, J., 2004. Estimating time since forest harvest using segmented Landsat ETM+ imagery. *Remote Sens. Environ.* 93, 179–187.
- Wulder, M.A., Coops, N.C., Roy, D.P., White, J.C., Hermosilla, T., 2018. Land cover 2.0. *Int. J. Remote. Sens.* 39, 4254–4284.
- Wulder, M.A., White, J.C., Bater, C.W., Coops, N.C., Hopkinson, C., Chen, G., 2014. Lidar plots — a new large-area data collection option: context, concepts, and case study. *Can. J. Remote. Sens.* 38, 600–618.
- Zald, H.S.J., Ohmann, J.L., Roberts, H.M., Gregory, M.J., Henderson, E.B., McGaughey, R.J., Braaten, J., 2014. Influence of lidar, Landsat imagery, disturbance history, plot location accuracy, and plot size on accuracy of imputation maps of forest composition and structure. *Remote Sens. Environ.* 143, 26–38.
- Zald, H.S.J., Wulder, M.A., White, J.C., Hilkert, T., Hermosilla, T., Hobart, G.W., Coops, N.C., 2016. Integrating Landsat pixel composites and change metrics with lidar plots to predictively map forest structure and aboveground biomass in Saskatchewan, Canada. *Remote Sens. Environ.* 176, 188–201.
- Zhu, Z., Woodcock, C.E., 2012. Object-based cloud and cloud shadow detection in Landsat imagery. *Remote Sens. Environ.* 118, 83–94.